Automated control of catalytic Janus micromotors

*Max Sokolich, David Rivas, Zameer Hussain Shah, Sambeeta Das**

Department of Mechanical Engineering, University of Delaware, Newark, DE 19716 USA

E-mail: samdas@udel.edu

Keywords: micromotors, magnetic-control, automation, Janus colloids

Abstract. Our study presents a highly accurate automated and human-free control mechanism for Janus micromotors powered by catalytic reactions. This system utilizes fully automated electromagnetic coils to direct the magnetic field toward a reference point, causing the particles to move in response to the catalytic decomposition of hydrogen peroxide. Magnetic torques without human intervention are applied to the particles, allowing them to align and move precisely. To ensure precise control, we have implemented algorithms that guide the particles to a desired location. In addition, a desired trajectory made up of multiple such points enables the active particles to move along more general and complex trajectories.

Introduction. Micromotors are tiny machines designed to perform specific tasks in complex environments [1-3]. The potential of these nanomachines is critical to shaping the future of effective biomedicine and a clean environment [4, 5]. However, further fundamental and applied research is necessary to realize their potential and ensure their safe and widespread use [6, 7]. On the fundamental side, understanding the active motion of micromotors is of prime significance [8]. Micromotors can be actuated by a chemical fuel such as peroxide or by an external source such as a magnetic field or light, etc. [9, 10]. Chemically powered micromotors have been the center of attention since their discovery in 2004 [11, 12]. These micromotors utilize fuel from their surroundings as a source of energy to drive their motion [13, 14]. Typically, these micron-sized particles are equipped with a catalyst to decompose the fuel [15]. In the classic design, polymeric microspheres are half-coated with platinum to fabricate asymmetric particles, also known as Janus colloids [16-18]. The non-symmetric nature of these particles results in an asymmetric breakdown of fuel molecules around the particle [19]. This non-uniform reaction around the particle results in an unequal pressure on the particle that leads to its directional motion via a self-phoretic effect [6, 17].

Even though chemically propelled particles demonstrate active motion, their direction is not controlled. For practical applications, it is highly desired to precisely control the micromotor motion from one point to another [20, 21]. To get control over the directionality, a magnetic component can be included in the chemically powered micromotor [22, 23]. This simple strategy allows the chemically powered micromotors to move in a specific direction under the influence of a magnetic field. However, human input in the form of controlling the magnetic signals is required [24]. In addition, currently there are limited modalities for real time

correction of the trajectories of such magnetically controlled micromotors. For most practical applications such as targeted therapy and micromanipulation, a point-to-point automated control of their motion is highly desired [25].

Previous attempts at using magneto-catalytic micromotors have generally been open-loop which requires human intervention [26]. For example, Palacci *et. al.* demonstrated that an active colloidal particle could be steered magnetically to a small cargo and then transport it to a targeted location [27]. Similarly, Baraban and co-workers reported that a weak homogeneous magnetic field could be used to control the direction of motion of Janus micromotors [28]. The weak magnetic fields have also been shown to control the motion and localization of Pt-SiO_2 Janus micromotors in 2D as well as 3D spaces [29]. In a more advanced model of magnetically controlled navigation, Joseph Wang's group have developed smart micromotors capable of semi-autonomous navigation in complex environments and traffic scenarios [30]. Despite these developments, a fully automated system capable of precise control over the motion of the catalytically powered micromotors with a self-regulating system is hard to come by [31].

A fully automated process involves a form of closed-loop control also known as feedback control. In feedback control, the response is continuously compared with the desired output and modified to minimize any deviations [31]. Closed-loop control has been utilized to control the motion of micromotors of different shapes [32]. Khalil and co-workers have extensively studied the closed-loop control of magnetically responsive chemically propelled microjets [33-35]. The authors controlled the orientation of the microjets with external magnetic torques while the linear motion towards a reference point was controlled by a thrust generated from the chemically produced oxygen bubbles and a magnetic field gradient created by the pulling magnetic forces. Similarly, Marino *et al* [36]. have reported the closed-loop control studies of cylindrical-shaped microbots. The authors presented different methods to control the uncertainties in electromagnetic force generation and drag forces. Recently, Jiang *et al* [37]. have developed a closed-loop control system to control the motion of a vortex-like magnetic microswarm. They employed commercial servo amplifiers to improve the performance of their system. However, a fully automated feedback control system for catalytic self-phoretic spherical micromotors has not yet been demonstrated.

To overcome this, we demonstrate a straightforward and minimal feedback control mechanism for automated control of 5 μm spherical catalytic Janus micromotors. We utilized a custom tracking program developed in Python and an in-house ModMag manipulation device [38]. Furthermore, the algorithm's efficacy was evaluated by executing complex trajectories that involved the micromotors tracing curved paths displayed on the video monitor.

Results and Discussion.

To investigate the movement of Janus micromotors, a suspension of particles (synthesis is provided in the Supplementary Information) was carefully deposited onto a glass substrate that had been thoroughly cleaned with plasma. Once the particles settled, a precise quantity of hydrogen peroxide (Fischer Scientific, 30%) was introduced to the particle layer. The addition of hydrogen peroxide triggered an immediate response from the particles, which began to move in an uncontrolled manner. The average speed of these micromotors was about 10 μm/s under our experimental conditions. This movement was achieved through the non-uniform chemical decomposition of hydrogen peroxide in the immediate vicinity of the particles, resulting in a propulsive force [9]. In the absence of a magnetic field, the micromotors followed curved trajectories. However, by applying magnetic torques, the direction of motion of the micromotors could be controlled. To generate uniform magnetic fields on the order of a mT, a custom-built electromagnetic coil system was used (details provided in Supplementary Information).

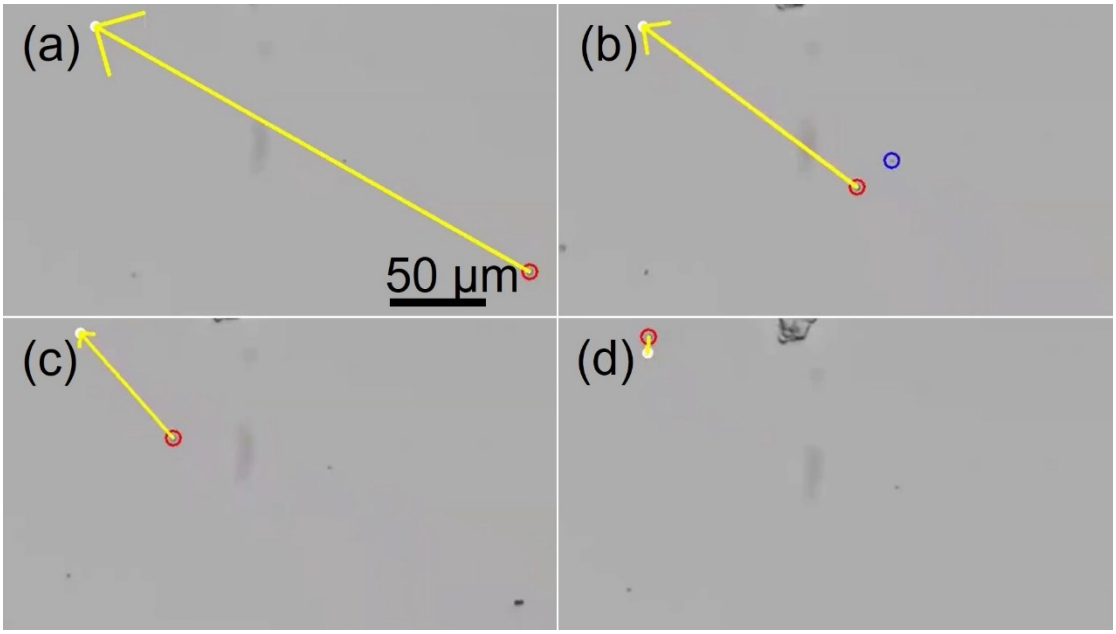

Figure 1. Time-lapse optical images of experimental trajectory of a 4.7 μm diameter micromotor. The red circle is the micromotor which was tracked by the algorithm, while the yellow arrow points from the micromotor to the desired target location. The blue circle in panel (b) was a piece of dust that the tracking algorithm identified within the moving search window. (a) At 1 sec, (b) 4 sec, (c) 8 sec, and (d) 11 sec (See video S1).

An applied magnetic field of 10 mT was used to control the direction of the active colloids. The micromotors had no preferred direction of motion when no magnetic field was applied which is consistent with the previous reports [39]. When a magnetic field is applied, the Janus

micromotors move in a straight line although their direction of motion is a priori unknown due to the angular offset between their magnetic moment vector and catalytic propulsion.

To achieve automated control over the directionality and position of the micromotors, a closed-loop control algorithm was developed. The algorithm (Algorithm 1) was used to determine the appropriate magnetic field direction based on the measured directional motion of the micromotor. Initially, a target location is selected and the directional motion of the micromotor is measured after applying an initial field direction in the x-direction (chosen arbitrarily). The relative angle between the direction of motion and the magnetic field is found and this is used to change the applied field direction via a rotational transformation in order to correct for this angular offset. The underlying logic of Algorithm 1 is depicted in Figure 3. When this control algorithm was applied to the micromotors, they were successfully guided to the target location, as shown in Figure 1 and video S1. Once the micromotors reached the target location, the code continues to adjust the magnetic field which keeps the micromotors in close proximity to the target location.

Algorithm 1 Catalytic Micromotor Closed Loop Control

input : target vector $\mathbf{t}$
output: Magnetic Field Vector $\mathbf{B}$

initialization
$\mathbf{B} \leftarrow [1, 0]$
while *True* **do**
  compute and store velocity $\mathbf{v}$
  if *N new frames:* **then**
    $\cos(\theta) \leftarrow \dfrac{\mathbf{v} \cdot \mathbf{B}}{\|\mathbf{v}\|\|\mathbf{B}\|}$
    $\sin(\theta) \leftarrow \dfrac{\mathbf{v} \times \mathbf{B}}{\|\mathbf{v}\|\|\mathbf{B}\|}$
    $\mathbf{T} \leftarrow \begin{bmatrix} \cos(\theta) & -\sin(\theta) \\ \sin(\theta) & \cos(\theta) \end{bmatrix}$
    $\mathbf{B} \leftarrow \mathbf{T}\mathbf{t}$
    apply B
  end
end

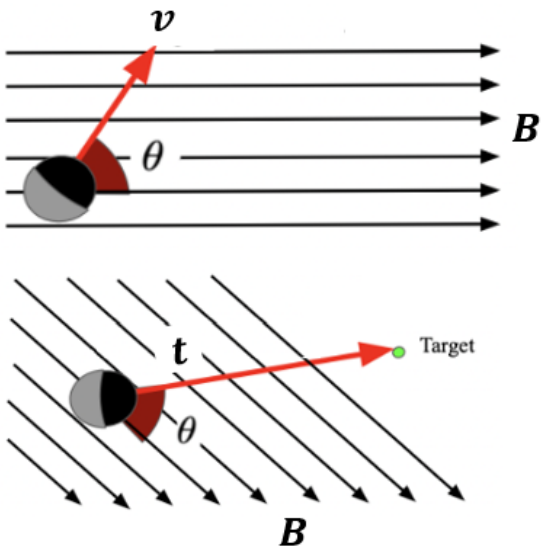

Figure 2. Algorithm 1. The black lines in the visual representation on the right-hand side represent applied magnetic field lines. Red lines indicate the micromotors velocity direction. Once a target location is selected by the user, the code applies a magnetic field that accounts for the angular offset between the field and the direction of micromotor motion.

Algorithm 1 takes inputs of the target vector, determined by the micromotor's location using Python code, such as "Trackpy" or open cv particle locating packages. The selected micromotor is continuously tracked, and the image is cropped around its center to reduce the search window for faster tracking. Therefore, search window continuously moves with the micromotor based on its location in the previous frame. The code computes the average velocity unit vector using the micromotor's previous N positions, with N chosen by the user. The target location is selected by right-clicking on the video display, and an initial magnetic field is applied. After N frames of tracking, the code corrects for the angular offset between the desired and actual directions of motion, using a transformation rotation matrix. The updated magnetic field vector is used to determine the current to apply to the coils, with the magnetic field direction being updated continuously.

We also created more complex trajectories for the micromotors to follow. Figure 4 and Video S2 demonstrates the ability of the algorithm to guide the micromotors along a curved trajectory. To acomplish this, the desired drawn trajectory was automatically broken down into individual nodes and the micromotor was directed to each node sequencially. A threshold distance that can be chosen by the user was used to determine if the micromotor had reached each node sucessfully. Figure 3 shows an outline of the algorithm used for guiding the micromotors along the multi-node trajectories. Algorithm 1 was still employed to direct the micromotors towards each node.

Algorithm 2 Nonlinear Closed Loop Trajectory Discretization

input : trajectory array of n nodes with positions (x,y)
output: Magnetic Field Vector $\mathbf{B} \leftarrow [B_x, B_y]$

initialization
$trajectory \leftarrow \left[[x_0, y_0]\ [x_1, y_1]\ [x_2, y_2]\ \cdots\ [x_n, y_n]\right]^T$
$n \leftarrow 0$;
while $n < len(trajectory)$ **do**
  $\mathbf{q} \leftarrow [p_x, p_y]$
  node $\leftarrow [x_n, y_n]$
  error $\leftarrow \sqrt{(x_n - p_x)^2 + (y_n - p_y)^2}$
  if ***error*** $<$ *threshold* **then**
    $n \leftarrow n + 1$
  else
    $B_x \leftarrow (x_n - p_x)$
    $B_y \leftarrow (y_n - p_y)$
    apply B

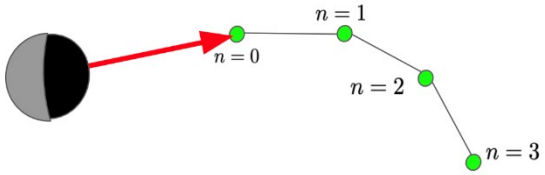

Figure 3. Algorithm 2. Green points represent nodes of the trajectory array and the red arrow indicates the micro-motors velocity vector. The micromotor is guided to each node in succession using Algorithm 1.

The above algorithm provides a versatile method for directing Janus micromotors to any target point and can be extended to guide them along desired trajectories. Algorithm 2 (Figure 3) enables the user to draw a desired trajectory on the video display using the cursor. The trajectory is then divided into multiple nodes, with the micromotor being guided to each node in succession. Algorithm 2 takes an array of points that describe the desired trajectory as input. The micromotor's position is determined relative to the target position using custom tracking software in python. The error between the robot's current position and the target node position is then calculated. If this error is less than a user-defined threshold value, the robot is considered to have arrived at the current node and can move on to the next node. If the error is greater than the threshold, then algorithm 1 is used to guide the micromotor toward the target node. Combining algorithm 1 and 2, we were able to direct the micromotors along non-linear trajectories, as illustrated in Figure 4 and video S2.

In order to measure the performance of this algorithm, we calculated the area between the desired and actual trajectories and divided it by the length of the desired trajectory squared. This results in a dimensionless number that we define as the Performance Metric (PM). A PM much less than one represents a trajectory that followed the desired path fairly well, while a PM that is not much less than one is not very precise. For the trajectories in Figure 4, the top trajectory has a PM of 0.01 and the bottom trajectory has a PM of 0.003 which indicates fairly good agreement between the actual and desired trajectories. Naturally, however, the desired

precision will depend on the requirements of the application.

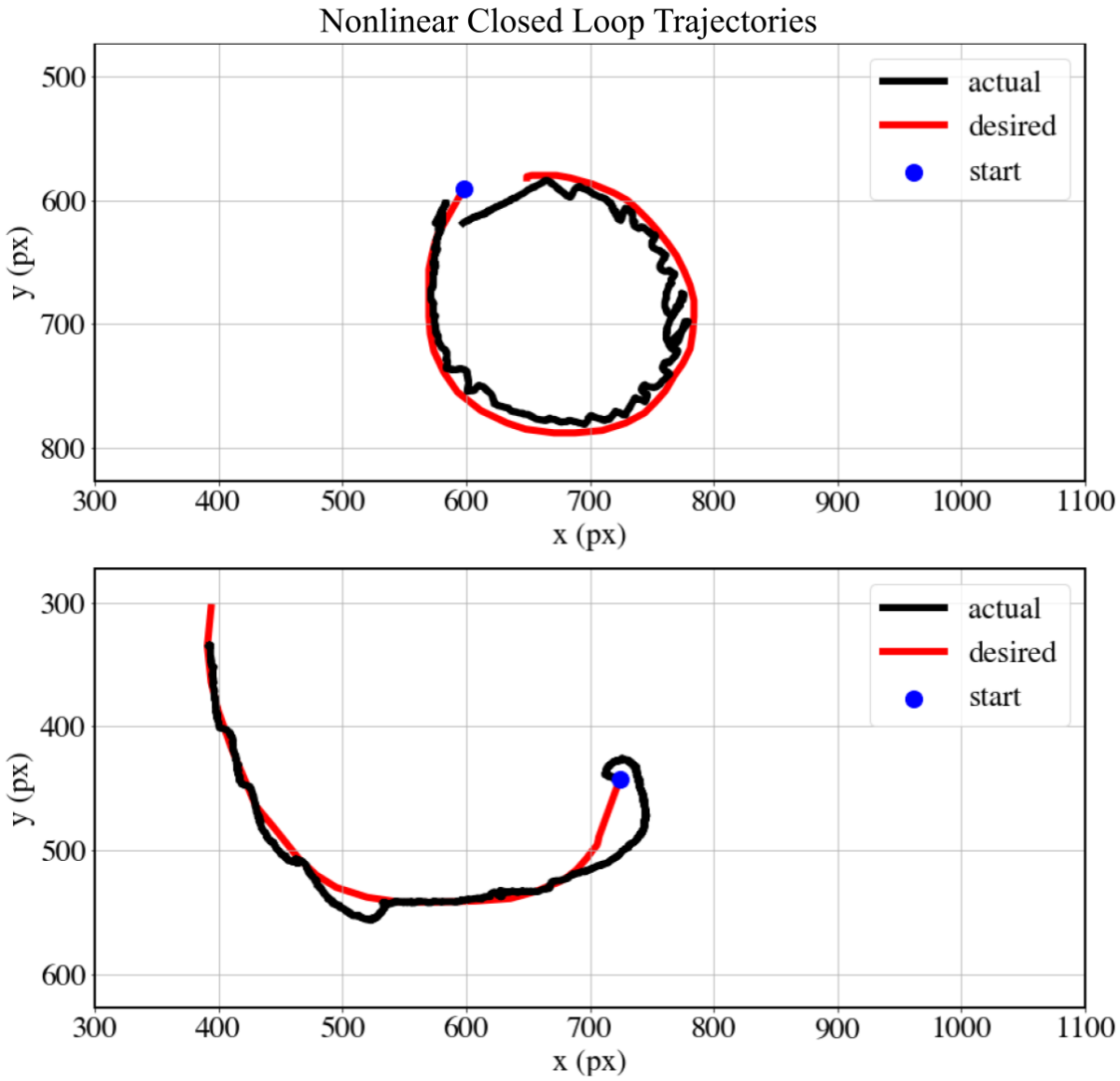

Figure 4. Two nonlinear trajectories implementing algorithm 1 and algorithm 2. The red curve indicates the desired trajectory defined by the user's right mouse click and the black curve indicates the actual trajectory of the micro-motor.

In general, Brownian motion and drift caused by fluid flow can result in deviations in the micromotors position. Because our micromotors moved at high Peclet number (defined as the ratio of self-propelled velocity to Brownian diffusion), Brownian motion was not a significant factor in these experiments. Also, drift was not observed since these experiments were conducted on a substrate where the bulk flows did not affect their motion. Since the algorithm continuously updates the applied field based upon the micromotor's current velocity, we expect that it would naturally compensate for these disturbances. However, future adjustments

to the algorithm could be made to specifically account for drift if it is significant compared to the micromotor's self-propelled velocity.

Conclusions. In summary, our study showcases a straightforward closed-loop control mechanism for chemically powered self-phoretic Janus micromotors. Our findings demonstrate that our magnetic arrangement and algorithms can successfully guide catalytically propelled Janus colloids with an unknown initial magnetic moment orientation towards a pre-defined target location. Our work is expected to be particularly beneficial in situations where precise control over particle movement is necessary. We have also demonstrated that the micromotors can follow user-drawn curved trajectories, in addition to more complex paths determined through path-planning, such as for obstacle avoidance. Overall, our closed-loop system offers promising potential for the practical applications of Janus micromotors.

Supplementary Information. The Supplementary Information contains schemes of microrobot synthesis and magnetic setup, SEM images of the micromotors, motion trajectory images, and videos showing the motion of micromotors.

Acknowledgments. This work is supported by an Institutional Development Award (IDeA) from the NIGMS of the National Institutes of Health under grant number U54-GM104941, from the NIGMS of the National Institute of Health under grant number 1R35GM147451, from the National Science Foundation under grant number 2020973 and from National Science Foundation under grant number 2218980. This content is solely the responsibility of the authors and does not necessarily represent the official views of NIH.

References

1 G. A. Ozin, I. Manners, S. Fournier-Bidoz, and A. Arsenault, Advanced Materials **17**, 3011 (2005).
2 T. Mirkovic, N. S. Zacharia, G. D. Scholes, and G. A. Ozin, Small **6**, 159 (2010).
3 S. Palagi and P. Fischer, Nature Reviews Materials **3**, 113 (2018).
4 J. Wang, *Nanomachines: Fundamentals and Applications* (John Wiley & Sons, 2013).
5 M. Safdar, S. U. Khan, and J. Jänis, Advanced Materials **30**, 1703660 (2018).
6 X. Chen, C. Zhou, and W. Wang, Chem. Asian J. **14**, 2388 (2019).
7 I. Santiago, Nano Today **19**, 11 (2018).
8 W. Wang, T.-Y. Chiang, D. Velegol, and T. E. Mallouk, J Am Chem Soc **135**, 10557 (2013).
9 Z. H. Shah, B. Wu, and S. Das, Front Robot AI **9**, 1027415 (2022).
10 C. Chen, F. Soto, E. Karshalev, J. Li, and J. Wang, Advanced Functional Materials **29**, 1806290 (2019).
11 T. Mirkovic, N. S. Zacharia, G. D. Scholes, and G. A. Ozin, ACS Nano **4**, 1782 (2010).
12 W. F. Paxton, K. C. Kistler, C. C. Olmeda, A. Sen, S. K. St. Angelo, Y. Cao, T. E. Mallouk, P. E. Lammert, and V. H. Crespi, J Am Chem Soc **126**, 13424 (2004).

[13] S. Sánchez, L. Soler, and J. Katuri, Angew. Chem. Int. Ed. **54**, 1414 (2015).
[14] W. Gao, S. Sattayasamitsathit, and J. Wang, The Chemical Record **12**, 224 (2012).
[15] Y. Zhang and H. Hess, Nature Reviews Chemistry **5**, 500 (2021).
[16] A. Sen, M. Ibele, Y. Hong, and D. Velegol, Faraday Discussions **143**, 15 (2009).
[17] W. Gao, A. Pei, R. Dong, and J. Wang, J Am Chem Soc **136**, 2276 (2014).
[18] W. Gao, M. D'Agostino, V. Garcia-Gradilla, J. Orozco, and J. Wang, Small **9**, 467 (2013).
[19] W. Gao, X. Feng, A. Pei, Y. Gu, J. Li, and J. Wang, Nanoscale **5**, 4696 (2013).
[20] Z. Yang and L. Zhang, Advanced Intelligent Systems **2**, 2000082 (2020).
[21] S. Das, A. Garg, A. I. Campbell, J. Howse, A. Sen, D. Velegol, R. Golestanian, and S. J. Ebbens, Nature Communications **6**, 8999 (2015).
[22] Y. Dong, et al., ACS Nano **15**, 5056 (2021).
[23] W. Gao, K. M. Manesh, J. Hua, S. Sattayasamitsathit, and J. Wang, Small **7**, 2047 (2011).
[24] E. Diller, S. Floyd, C. Pawashe, and M. Sitti, IEEE Transactions on Robotics **28**, 172 (2012).
[25] J. E. Wu, et al., Advanced Intelligent Systems **4**, 2200192 (2022).
[26] H. Zhou, C. C. Mayorga-Martinez, S. Pané, L. Zhang, and M. Pumera, Chemical Reviews **121**, 4999 (2021).
[27] J. Palacci, S. Sacanna, A. Vatchinsky, P. M. Chaikin, and D. J. Pine, J Am Chem Soc **135**, 15978 (2013).
[28] L. Baraban, D. Makarov, O. G. Schmidt, G. Cuniberti, P. Leiderer, and A. Erbe, Nanoscale **5**, 1332 (2013).
[29] I. S. M. Khalil, V. Magdanz, S. Sanchez, O. G. Schmidt, and S. Misra, International Journal of Advanced Robotic Systems **12**, 2 (2015).
[30] T. Li, et al., ACS Nano **11**, 9268 (2017).
[31] K. L. S. Sharma, in *Overview of Industrial Process Automation*, edited by K. L. S. Sharma (Elsevier, London, 2011), p. 53.
[32] X. Wu, J. Liu, C. Huang, M. Su, and T. Xu, IEEE Transactions on Automation Science and Engineering **17**, 823 (2020).
[33] I. S. M. Khalil, V. Magdanz, S. Sanchez, O. G. Schmidt, and S. Misra, IEEE Transactions on Robotics **30**, 49 (2014).
[34] I. S. M. Khalil, V. Magdanz, S. Sanchez, O. G. Schmidt, and S. Misra, Applied Physics Letters **103**, 172404 (2013).
[35] I. S. M. Khalil, V. Magdanz, S. Sanchez, O. G. Schmidt, and S. Misra, PLOS ONE **9**, e83053 (2014).
[36] H. Marino, C. Bergeles, and B. J. Nelson, IEEE Transactions on Automation Science and Engineering **11**, 310 (2014).
[37] J. Jiang, L. Yang, and L. Zhang, IEEE Robotics and Automation Letters **6**, 827 (2021).
[38] M. Sokolich, D. Rivas, Y. Yang, M. Duey, and S. Das, MethodsX **10**, 102171 (2023).
[39] J. R. Howse, R. A. L. Jones, A. J. Ryan, T. Gough, R. Vafabakhsh, and R. Golestanian, Physical Review Letters **99**, 048102 (2007).